Journal of Catalysis **197,** 182–191 (2001)
doi:10.1006/jcat.2000.3073, available online at http://www.idealibrary.com on IDEAL®

# Flame Aerosol Synthesis of Vanadia–Titania Nanoparticles: Structural and Catalytic Properties in the Selective Catalytic Reduction of NO by $NH_3$

Wendelin J. Stark,*,† Karsten Wegner,† Sotiris E. Pratsinis,† and Alfons Baiker*

*Laboratory of Technical Chemistry and †Institute of Process Engineering, ETH Zentrum, CH-8092 Zurich, Switzerland

Received June 28, 2000; revised September 19, 2000; accepted September 19, 2000

**Flame aerosol synthesis has been used to prepare vanadia–titania nanoparticles with high activity for the selective catalytic reduction of NO by $NH_3$. The mixed oxides were prepared from vanadium and titanium alkoxides which were evaporated into an argon stream and burned in a methane oxygen diffusion flame. Silica-containing samples were produced in a similar way by mixing hexamethyldisiloxane vapor into the precursor stream. Different flame structures were investigated for the effect of temperature and residence time on particle morphology, vanadia surface species, and overall catalytic activity. By changing the oxygen flow rate into the flame, particles with specific surface areas between 23 and 120 $m^2/g$ could be produced. High-resolution transmission electron microscopy (HRTEM) revealed that nanoparticles were spherical with diameters of 10 to 50 nm. X-ray photoelectron spectroscopy analysis indicated that vanadia was dispersed on the surface of the titania spheres. No indication for the presence of crystalline $V_2O_5$ could be found by X-ray diffraction or HRTEM. Catalysts with a vanadia surface loading of 10 $\mu mol/m^2$ showed high activity with less than 1% $N_2O$ formation up to 350°C. Catalytic activity strongly depended on the vanadia loading; an increase from 2.5 to 7 $\mu mol/m^2$ resulted in a 30 times higher activity per vanadium. Addition of silica lowered the overall activity but did not change the activation energy. Raman spectroscopy indicated the presence of vanadate clusters. Temperature-programmed reduction corroborated that no significant amount of vanadia entered the titania lattice to form an interstitial solution. The selective catalytic reduction activity of as-prepared vanadia–titania is comparable to the best catalysts obtained by wet chemical methods.** 

*Key Words:* **flame; aerosol; vanadia; titania; silica; selective catalytic reduction; nitrogen oxide; ammonia; nanoparticles.**

## 1. INTRODUCTION

Flame aerosol synthesis is widely used in industry for the manufacture of fumed silica, carbon-blacks, and pigmentary titania as well as other oxides (1). Careful adjustment of temperature, residence time, and precursor concentration allows the production of nanoparticles with well-controlled properties on an industrial scale (2). Flame aerosol synthesis uses a volatile precursor that is burned in a flame. Initially formed oxide vapor and clusters quickly condense and form ceramic nanoparticles which further grow by coagulation and coalescence. This is attractive for the manufacture of catalysts as the specific surface area and the crystallinity can be controlled independently in the gas phase (1, 3).

Little work has been done so far on the use of aerosols for catalytic applications, even though Ulrich (3) had already suggested the use of flame aerosol synthesis to produce catalysts in 1984. Moser (4) used a high-temperature aerosol decomposition process to produce bismuth molybdate, noble metals on alumina, phosphorous vanadium oxide, and some perovskites. The vanadium phosphorous oxide powder (VPO) was produced between 350 and 800°C by pyrolysing a phosphoric acid containing ammonium vanadate solution in a hot wall reactor. Residence times were around 8 s and specific surface areas were rather low, typically 6–14 $m^2/g$. The powders were active in butane oxidation, but consisted of a different phase than the classical catalyst (4). Michalakos *et al.* (5) used spray pyrolysis also to produce a VPO catalyst with better selectivity to maleic anhydride and higher activity per mass than the corresponding materials from conventional methods. Moser (6) reported exceptional dispersion for noble metals on alumina, but specific surface areas were only around 10 $m^2/g$. A $LaFeO_3$ perovskite was active in Fischer Tropsch synthesis (7). Miquel and Katz (8) synthesized vanadium pyrophosphate in a counter-flow diffusion burner from the corresponding halides. Titania with 14, 25, and 50 wt% vanadia and pure $V_2O_5$ were made in a hydrogen oxygen flame using $VOCl_3$ and $TiCl_4$ as precursors (9). However, no activity measurements were reported in both cases. Composite titania/silica particles prepared with the same burner showed a wide variety of structures (10). Fotou *et al.* (11, 12) showed that titania made in a diffusion flame reactor exhibits better photocatalytic performance than Degussa P25 in the decomposition of phenol and salicylic acid.

In this study, a methane oxygen coflow diffusion flame is used to produce vanadia–titania nanoparticles. Vanadia–titania-based catalysts are widely applied for the selective



0021-9517/01 $35.00

catalytic reduction (SCR) of NO by $NH_3$ (13). This prompted us to choose SCR as a test reaction for elucidating the catalytic properties of the new material. Chemical and structural properties are investigated using laser ablation ion coupled plasma mass spectroscopy (L-ICP-MS), temperature-programmed reduction (TPR), X-ray diffraction (XRD), nitrogen adsorption, high-resolution transmission electron microscopy (HRTEM), X-ray photoelectron spectroscopy (XPS), and Raman spectroscopy.

## 2. EXPERIMENTAL

### 2.1. Catalyst Preparation

A coflow-diffusion burner is used for aerosol synthesis of vanadia–titania nanoparticles. The experimental setup is shown in Fig. 1. The reactor consisted of three concentric stainless-steel tubes with inner diameters of 2.5, 4.0, and 5.5 mm and a wall thickness of 0.3 mm. An argon stream of 1.5 L/min carrying the precursor vapor was introduced through the center tube and methane flowed through the inner annulus at a rate of 0.5 L/min, while oxygen was provided through the outer annulus, resulting in a simple diffusion flame (14). Different experiments were performed with oxygen flow rates of 2 to 10 L/min. Figure 2 depicts typical flames producing vanadia–titania nanoparticles. All gases (Pan Gas, purity >99.999%) were delivered from cylinders with the flow rates monitored by calibrated mass flow controllers (Bronkhorst EL-Flow F201). Mixtures of titanium–tetra-isopropoxide (Aldrich, >97%) and vanadium–oxo-tri-isopropoxide (Aldrich, >97%) were prepared and stored under argon. The mixture was fed to an evaporator (E1 in Fig. 1, Bronkhorst CEM 100 W) at a flow rate of 13 g/h controlled by a liquid mass flow meter (Bronkhorst Liqui-Flow L1) and evaporated into an argon stream of 1.0 L/min. A second evaporator (E2) was used to vaporize iso-octane ($C_8H_{18}$, Fluka, >99.5%) at a flow rate of 2.4 g/h into an argon stream of 0.5 L/min. For samples containing silica, some of the iso-octane was substituted by the equivalent amount of hexamethyldisiloxane (HMDSO, Fluka, >99%). Since iso-octane and HMDSO have a similar heat of combustion (−5895 kJ/mol for HMDSO and −5469 kJ/mol for iso-octane), the fuel content in the flame was constant throughout all experiments (15). Both evaporators, the precursor delivery tubes, and the burner were heated to 150°C to prevent condensation of the precursor vapor. The flame was surrounded by a quartz chimney (glass cylinder, id = 140 mm) in order to achieve stable burning. A stainless-steel filter holder with a glass fiber filter (Whatman GF/A) was mounted on top of the cylinder. Product particles were collected on the filter with the aid of a vacuum pump (Vacuubrand RE 5). Each experiment was reproduced at least twice. The different materials are designated as *x*V*y*Si*z*, were *x* and *y* denote the weight fractions of vanadia and silica, respectively, and *z* is the oxygen flow rate applied in liters per minute.

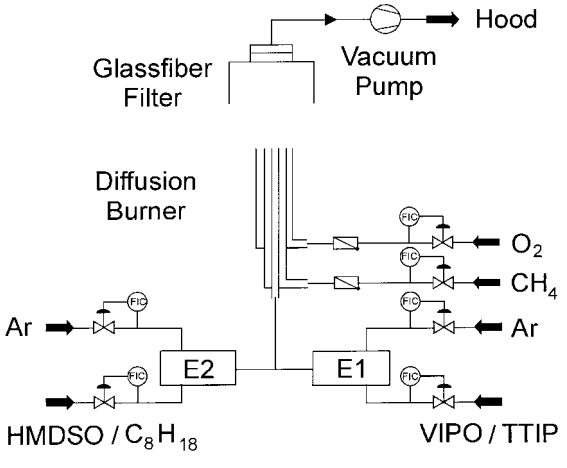


**FIG. 1.** Schematic of flame aerosol reactor setup (E1, E2: evaporators).

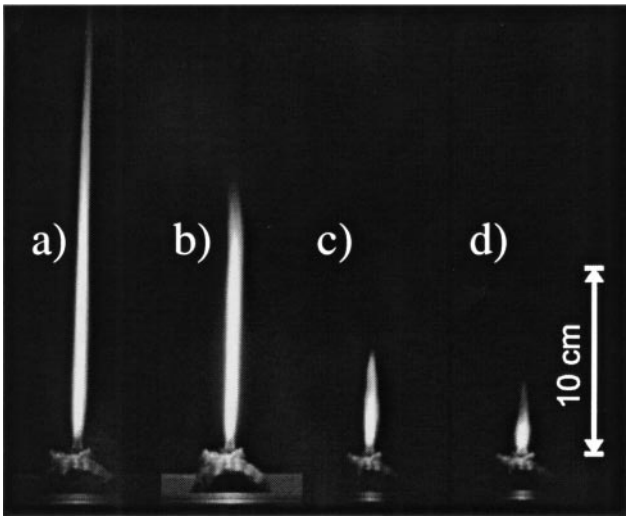


**FIG. 2.** Flames producing titania–vanadia nanoparticles at oxygen flow rate = 2, 3, 6, and 10 L/min (a to d). Flow rates of methane and argon: 0.5 and 1.5 L/min.

### 2.2. Catalyst Characterization

*Specific surface area (SSA) and isotherms.* The SSA of the collected powders was analyzed by nitrogen adsorption at 77 K using the BET method (Micrometrics GEMINI 2360). The results were cross-checked by recording a full adsorption isotherm (Micrometrics ASAP 2010 Multigas system).

*High-resolution transmission electron microscopy.* The HRTEM investigations were performed with a CM30ST microscope (Philips; $LaB_6$ cathode, operated at 300 kV, point resolution ∼2 Å). Particles were deposited onto a carbon foil supported on a copper grid.

*Laser Raman spectroscopy.* Raman spectra of all catalysts were measured with the 647-nm line of a Krypton laser (Innova 300, Coherent) using a confocal Raman microscope (Labram, Dilor Instruments S.A.). The laser light was guided through a microscope (Olympus BH-2) on the sample which was pressed to 1-mm-thick plates prior to analysis. The focus of the microscope was adjusted by a video camera inserted in the ocular. The backscattered or reflected light passed through a holographic filter (Notch filter) on the pin hole of a monochromator (Spex, Model 14018). The detection was done with a Peltier-cooled CCD camera (EEV, $300 \times 1200$ pixel). The diameter of the focused laser beam was about 20 $\mu$m. Spectra were recorded at different laser energies between 200 $\mu$W and 5 mW to ensure that no changes of the sample occurred during measurement. Spectra of all catalysts were recorded at 1 mW during 15 min. Initial and final scans overlapped completely, indicating that no modifications of the sample occurred. No changes in color were observed after measurement. For all scans, the spectral resolution and reproducibility was better than 4 $cm^{-1}$.

*X-ray photoelectron spectroscopy.* All XPS spectra were recorded on an ESCALAB 220I XL (VG-Scientific) with an Al anode (Al $K_\alpha$, $h\nu = 1486.6$ eV) at a power consumption of 100 W. Chamber pressures were below $5 \times 10^{-9}$ mbar. The position of the C 1s and the Ti 2p 3/2 was used to account for charging effects (16). The vanadia and silica contents were determined using the method of Scofield (17).

*X-ray diffraction.* The XRD patterns of all powders were obtained at room temperature using a Siemens D5000 diffractometer operating with Cu($K_\alpha$) radiation. Particle size estimates were obtained by using the {101} reflection for anatase. The angle, $\Theta$, at which the peak maximum occurred, the full width at half maximum intensity, FWHM, and the wavelength, $\lambda$, of the copper radiation were inserted into the Scherrer equation $d_c = 0.9\lambda/\beta \cos\Theta$ to obtain the mean dimension of the crystallites, $d_c$. $\beta$ represents the corrected FWHM according to $\beta = (\mathrm{FWHM}^2 - B^2)^{0.5}$, where the instrumental broadening, $B$, is equal to 0.08.

*Laser ablation ion coupled plasma mass spectrometry.* Samples were pressed to plates and shot at with an Excimer laser (Compex 110 I, 193 nm, ArF, Lambda Physik; pulse energy 150 mJ, frequency 10 Hz) at a spot diameter of 40 $\mu$m. The vaporized sample was carried by a helium stream to a quadrupole ICP mass spectrometer (Elan 6100, Perkin–Elmer) and analyzed for all 3d-metals and silicon. Calibration was done with NIST 610 glass standards. Details are given in Ref. (18).

*Temperature-programmed reduction.* The TPR measurements were run in an apparatus described in detail in Ref. (19). The conditions used were sample weight 0.15 g; reduction gas 5% $H_2$/He at 30 ml/min; heating rate 10 K/min; temperature range 50 to 1000°C. Materials were oxidized in air at 450°C for 30 min prior to reduction.

### 2.3. Catalytic Tests

The catalytic behavior of the materials in SCR of NO by $NH_3$ was tested in a continuous flow fixed bed microreactor (20) in the temperature range between 90 and 390°C. Catalyst samples of 0.125 ml, pressed at 20 bar for 3 min and sieved to a fraction between 0.12 and 0.3 mm in diameter, typically were about 70 mg (21). All catalysts were heated *in situ* to 450°C under flowing air for 1 h, cooled to room temperature, and heated in SCR feed gas (15 ml/min, 900 ppm NO, 900 ppm $NH_3$, 1.8% $O_2$ in helium) to 400°C for 30 min to ensure that no structural or chemical changes occurred during the catalytic testing. No structural changes were observed in XRD during this pretreatment step. The testing sequence consisted of temperature steps of 15°C. At each step, the reactor was kept for 1 h to establish steady-state conditions. Concentrations of the product gases (NO, $NO_2$, $NH_3$, $H_2O$, $N_2O$, $O_2$) were monitored quantitatively with a quadrupole mass spectrometer (Balzers QMA 425). Conversion measurements as a function of temperature were carried out at an hourly space velocity of 24,000 $h^{-1}$. Kinetic parameters (turnover frequency, TOF, and activation energy, $E_a$) were determined differentially, keeping the conversion within 15 to 20% by changing the space velocity from 17,000 to 85,000 $h^{-1}$ and adjusting the temperature. Selectivities to $N_2$ and $N_2O$ are defined as $S_i = F_i/(F_{N_2} + F_{N_2O})$, where $F_i$ is the molar flow rate (mol/s) of species $i$ ($N_2$ or $N_2O$) at the reactor outlet. For all measurements a nitrogen balance including feed and product stream concentrations of all nitrogen containing species was calculated. Even at high conversions, the error in the N balance did not exceed 3%.

## 3. RESULTS

### 3.1. Structural and Textural Properties

*Laser ablation ICP-MS.* The elemental composition of six powders with different silica content produced at oxygen flow rates of 3 and 6 L/min is listed in Table 1. The vanadia content was found to be almost independent of the preparation method, showing that the composition of the precursor mixture was preserved. No vanadia was lost in the gas phase during the powder production and collection on the filter. Low oxygen flow rates, however, led to a slightly lowered vanadia content. Silica content was not affected by the flame structure and remained constant throughout all experiments. No soot formation was observed in any experiment.

*Specific surface areas.* The specific surface areas of all materials are listed in Table 1 and further compared in Fig. 3. The SSA is a strong function of the flame structure. A

**TABLE 1**

**Preparation Conditions and Catalyst Compositions**

| Sample | $O_2$ flow/ L min$^{-1}$ | Flame length/cm | V content/ wt% | V loading/ $\mu$mol m$^{-2}$ [c] | Si content/ wt% | $S_{BET}$/ m$^2$g$^{-1}$ [d] | XRD analysis[e] | $\langle d_c \rangle$/nm |
|---|---|---|---|---|---|---|---|---|
| 10V10 | 10 | 2.5 | 10[b] | 9.2 | 0 | 120 | A, R | 13 |
| 10V8 | 8 | 3.5 | 10[b] | 12.4 | 0 | 90 | A, R | 16 |
| 10V6 | 6 | 5 | 10.2[a] | 14.4 | 0 | 76 | A, R | 18 |
| 10V3 | 3 | 7 | 9.7[a] | 22 | 0 | 49 | A | 23 |
| 10V2 | 2 | 22 | 10[b] | 47.8 | 0 | 23 | A | 30 |
| 5V6 | 6 | 5 | 5[b] | 7.0 | 0 | 82 | A, R | 18 |
| 2V6 | 6 | 5 | 2[b] | 2.5 | 0 | 88 | A, R | 17 |
| 0V6 | 6 | 5 | 0[b] | 0 | 0 | 74 | A, R | 18 |
| 10V4Si6 | 6 | 5 | 10.6[a] | 13.7 | 3.6[a] | 80 | A, R | 18 |
| 10V4Si3 | 3 | 7 | 10.5[a] | 23.1 | 3.6[a] | 48 | A | 23 |
| 10V7Si6 | 6 | 5 | 9.9[a] | 13.6 | 7.2[a] | 80 | A, R | 18 |
| 10V7Si3 | 3 | 7 | 9.3[a] | 23.4 | 7.2[a] | 47 | A | 23 |
| 5V3 | 3 | 7 | 5[b] | 10.1 | 0 | 55 | A | 22 |

*Note.* Methane flow: 0.5 L/min; argon flow: 1.5 L/min.
[a] Measured by laser ablation ICP MS.
[b] Nominal content.
[c] Assuming all vanadia stays on the surface.
[d] Error ±3%.
[e] A, anatase; R, rutile. Rutile content in all samples was below 10%.

laminar flame (Fig. 2a) with an oxygen flow rate of 2 L/min leads to an SSA of 23 m$^2$/g in the case of titania particles with 10 wt% vanadia. Particles of the same composition showed a specific surface area of 120 m$^2$/g when they were produced in a turbulent flame (Fig. 2d) with an oxygen flow rate of 10 L/min. The influence of vanadia content on the SSA is demonstrated in Fig. 3 for powders produced at a constant oxygen flow rate of 6 L/min. Addition of 2, 5, and 10 wt% vanadia to titania had very little effect on the SSA. Addition of 3.6 and 7.2 wt% silica to particles with 10 wt% vanadia produced in flames with oxygen flow rates of 3 and 6 L/min had almost no influence on the SSA, as can be seen from Table 1. Specific surface areas were about 80 m$^2$/g for the 6-L flames and 48 m$^2$/g for the 3-L flames. Figure 4 depicts a typical isotherm (a) and the corresponding *t*-plot (b) of flame-made powders. According to IUPAC nomenclature, it can be classified as a type IV isotherm with a weak hysteresis. The *t*-plot clearly indicates only marginal micropores which could stem from agglomeration of the nanoparticles.

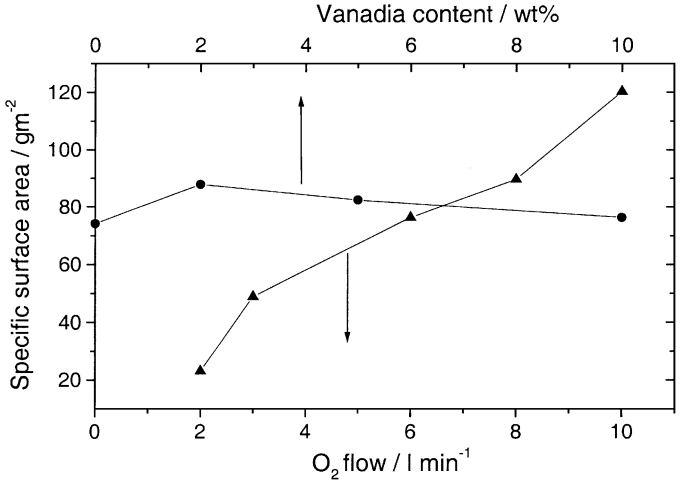


**FIG. 3.** Specific surface area (BET) as a function of $O_2$ flow rate (triangles) at 10 wt% vanadia content and vanadia content (circles) at constant 6 L $O_2$/min. Increased $O_2$ flow rates lead to steeper temperature gradients and faster cooling. Vanadia does not influence the specific surface area.

*X-ray diffraction.* The XRD patterns of titania with 10% vanadia are given in Fig. 5a as a function of oxygen flow rate during preparation. All samples show the characteristic reflections of anatase. Small amounts of rutile form in oxygen-rich flames (10V6, 10V8, 10V10), indicated by a small reflection at 27°. Crystallite sizes were considerably smaller at high oxygen flow rates, as indicated by line broadening in agreement with SSA measurements (Table 1). XRD patterns of samples containing silica are compared in Fig. 5b. No silica phase could be detected in any sample, indicating that silica is X-ray amorphous. Silica does not affect rutile formation in this flame, since both 10V6 and 10V7Si6 contained similar amounts of rutile. The 3-L flame samples 10V3 and 10V7Si3 do not show any rutile at all. None of the samples shown in Figs. 5a and 5b contained $V_2O_5$ or any other vanadium oxide in crystalline form. Samples synthesized in a 6-L flame with different vanadia content (0V6, 2V6, 5V6, and 10V6) showed the same amount of rutile, indicating that vanadia did not have a detectable effect on the anatase-to-rutile ratio.

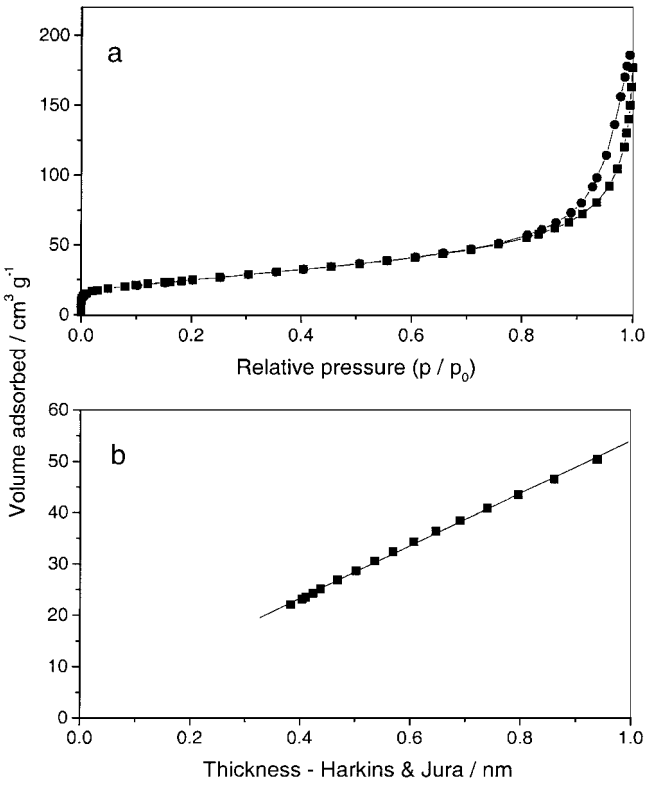


**FIG. 4.** (a) Isotherm and (b) corresponding *t*-plot of a typical flame-made catalyst (10V8).

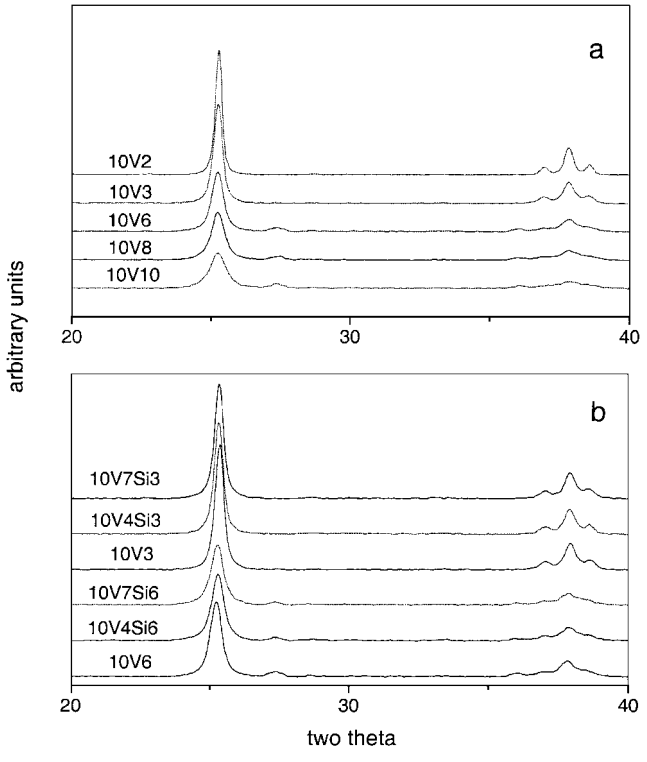


**FIG. 5.** XRD patterns of 10 wt% vanadia samples prepared (a) with different oxygen flow rates and (b) with different silica content and oxygen flow rates of 3 and 6 L/min.

**TABLE 2**

**TPR Results, after Air Pretreatment**

| Sample | Nominal V content/wt%[a] | $T_{max}$/K[b] | Relative $H_2$ uptake[c] |
|---|---|---|---|
| 10V10 | 10 | 767 | 1.0 |
| 2V6 | 2 | 733 | 0.20 |
| 10V2 | 10 | 791; 915; 1030 | 0.95 |
| EL10V1[d] | 1 | 783; 813 | 0.11 |
| EL10V8[d] | 8 | 833; 913 | 0.80 |

[a] As given by precursor composition.
[b] Estimated error, 10 K.
[c] Hydrogen consumption related to that of 10V10 (estimated error 5%).
[d] Taken from (19).

*Temperature-programmed reduction.* Relative hydrogen consumption and temperature of maximal hydrogen consumption rate $T_{max}$ are listed in Table 2 and compared with Eurocat samples (19). Reduction occurred at slightly lower temperatures. The relative hydrogen consumption correlates with the L-ICP-MS data. 10V10 and 2V6 showed only one reduction peak, whereas sample 10V2 exhibited three peaks. The first signal, contributing about 80% of total hydrogen consumption, occurred at the same temperature as in other vanadia catalysts, whereas the second consumed about 15% of hydrogen and coincided with a peak observed for the Eurocat EL10V8. The last signal at 1030 K contributing the remaining 5% has not been found in other catalysts.

*High-resolution transmission electron microscopy.* HRTEM pictures of the catalysts 10V6 and 10V7Si6 are given in Figs. 6 and 7. Flame-generated titania formed small spheres with diameters from 10 to 50 nm. Lattice fringes are discernible up to the surface of the particles corroborating their monocrystalline structure. There is no indication where the vanadia is located. Silica forms individual domains in agreement with the findings of Hung and Katz (10).

*X-ray photoelectron spectroscopy.* Surface concentrations of vanadia and silica of samples 10V6, 10V3, and 10V7Si6 are given in Table 3. Assuming an average penetration depth, a mass balance for silica and vanadia can be calculated, showing that vanadia and silica were located on the surface of the titania spheres. The 10V3 catalyst had a higher vanadium surface concentration due to its lower SSA than 10V6. Two distinct O(1s) signals were visible in

**TABLE 3**

**Surface Composition**

| Sample | V content/wt% | Ti content/wt% | Si content/wt% |
|---|---|---|---|
| 10V6 | 26.8 | 73.2 | — |
| 10V3 | 29.4 | 70.6 | — |
| 10V7Si6 | 20.6 | 54.9 | 24.5 |

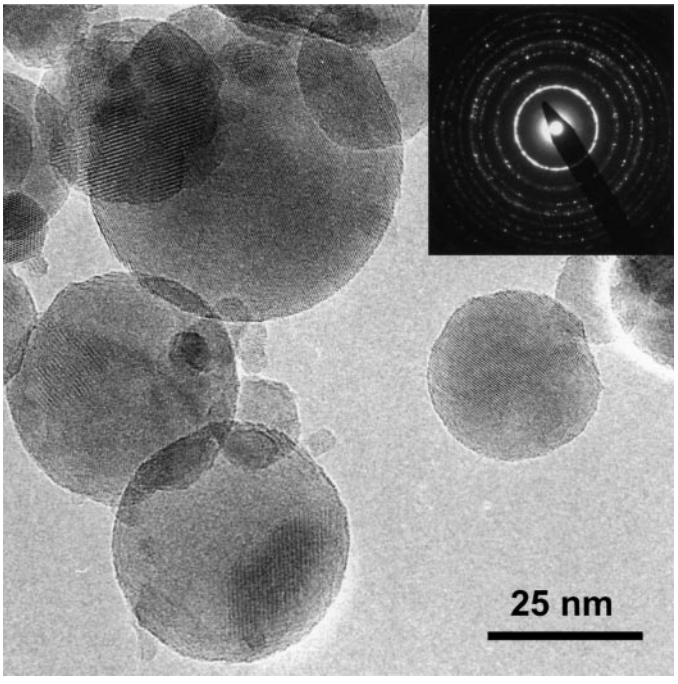


**FIG. 6.** HRTEM micrograph of sample 10V6 with diffraction pattern. The diffraction spacing clearly indicates the presence of crystalline anatase. Lattice planes are discernible in several particles.

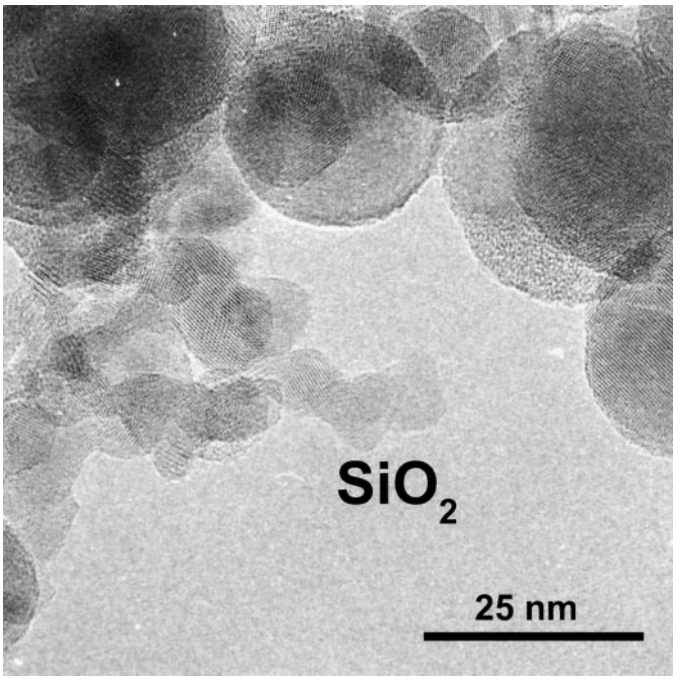


**FIG. 7.** HRTEM micrograph of sample 10V7Si6. Silica and titania form two separate phases.

silica-containing samples; the ratio of the latter corresponded to the silica-to-titania ratio.

*Laser Raman spectroscopy.* Raman spectra of powders with 10 wt% vanadia are presented in Fig. 8 as a function of the oxygen flow rate into the particle-generating flame. Distinct signals seen in the 720- to 1180-$cm^{-1}$ region of the spectrum of a powder produced at low oxygen flow rates (10V2) are a peak at 993 $cm^{-1}$, a shoulder at 1020 $cm^{-1}$, and a broad signal around 900 $cm^{-1}$. The band at 993 $cm^{-1}$ indicates the formation of microcrystalline $V_2O_5$ (22). The shoulder at 1020 $cm^{-1}$ is attributed to the presence of small amounts of monomers according to the literature (23–26). The broad signal around 900 $cm^{-1}$ may be assigned to a series of polymeric vanadates (23). Increasing the oxygen flow rate to 3 L/min produced vanadia partially in the form of monomers, indicated by a shoulder at 1020 to 1030 $cm^{-1}$ in the spectrum of 10V3. A lower intensity of the signal at 993 $cm^{-1}$ indicated less crystalline $V_2O_5$. The spectra of powders produced at oxygen flow rates of 6, 8, and 10 L/min (10V6, 10V8, and 10V10) showed a less distinct shoulder around 1020 $cm^{-1}$ and a more pronounced band around 900 $cm^{-1}$. This indicates that the monomer concentration slightly decreased and vanadia predominantly existed as polymeric vanadates. The origin of a series of signals around 800 $cm^{-1}$ is unclear.

Raman spectra of powders synthesized under similar conditions in a 6-L flame are shown in Fig. 9 as a function of vanadia content. Small amounts of vanadia present in the 2V6 sample predominantly showed signals of oligomers, as indicated by the broad signal around 940 $cm^{-1}$, not present in the spectrum of pure titania 0V6. A shoulder attributed to monomers is not observed. In the 5% vanadia sample (5V6), the signal of the polymeric vanadia increased and shifted to lower wavenumbers, as has been observed earlier (23). The sample 10V6, having the highest vanadia content in this series, showed signals of monomers, oligomers, and crystalline vanadia. The bands below 860 $cm^{-1}$ could not be clearly assigned.

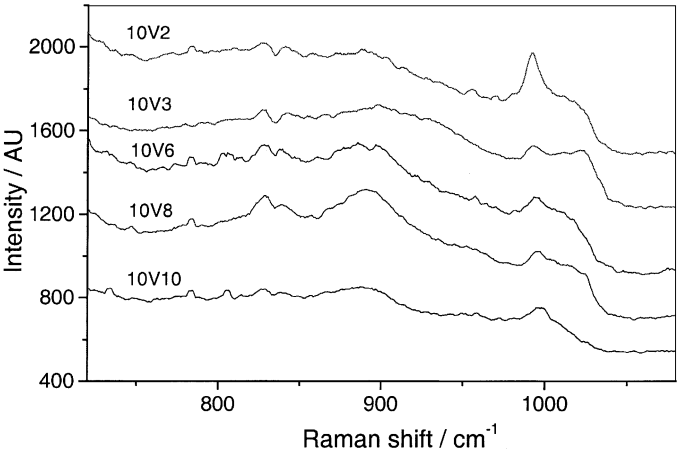


**FIG. 8.** Raman spectra of materials containing 10 wt% vanadia prepared under different conditions. Oxygen flow rates vary from 2 (top) to 10 L/min (bottom).

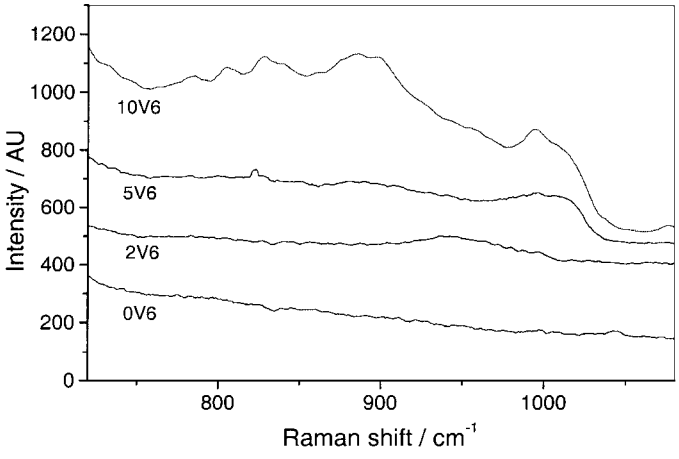


**FIG. 9.** Raman spectra of materials with different vanadia content but similar specific surface area.

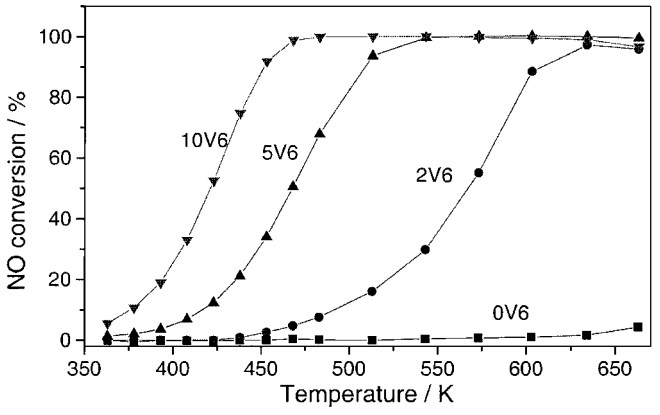


**FIG. 10.** NO conversion of samples with different vanadia content as a function of temperature at a global hourly space velocity of 24,000 h$^{-1}$.

### *3.2. Catalytic Performance*

Figure 10 gives the NO conversion as a function of temperature for samples with different vanadia contents. The titania support (0V6) was almost inert and showed less than 5% conversion up to 663 K. The low vanadia sample 2V6 had a $T_{50}$, the temperature where 50% of NO is converted, above 560 K (Table 4). The 5V6 powder was considerably more active and showed a $T_{50}$ of 468 K. The temperature dependence of the NO conversion was similar to the 10V6 sample with a $T_{50}$ of 421 K. Figure 11 depicts the NO conversion as a function of temperature for materials produced with various oxygen flow rates. The maximum activity was found for the 10V10 powder, synthesized with an oxygen flow rate of 10 L/min. More than 99% NO conversion was obtained between 473 and 633 K. The selectivity to $N_2O$ strongly varied for different preparation conditions. The sample 10V2 showed 60% $N_2O$ formation at 663 K. The selectivity to $N_2O$ decreased considerably when powders were produced at high oxygen flow rates. Selectivity to $N_2$ was better than 99% for 10V10, 10V8, and 10V6 up to 573 K. For materials made with less than 6 L/min oxygen, up to 25% NO was formed again at high temperatures reducing the NO conversion. For an SCR application the sample 5V3 may be the most interesting, as a TOF value of 3.2 ks$^{-1}$ at 473 K and less than 1% $N_2O$ formation up to 623 K opens a broad working window.

Figure 12a presents the Arrhenius plots for catalysts with different vanadia contents. The activation energy decreased from 92 to 60 kJ/mol with increasing vanadia content from 2 to 10 wt%. Arrhenius plots for powders with different silica content prepared in 3- and 6-L flames are depicted in Fig. 12b. The activation energy was not affected by the addition of silica and remained at 60 kJ/mol. Adding 3.6 wt%

**TABLE 4**

**Catalytic Activity: TOF; Reaction Rate Related to Surface $r_s$ and to Catalyst Mass $r_m$**

| Sample | TOF/ks$^{-1}$ at 473 K | $10^9 r_s$/ mols$^{-1}$ m$^{-2}$ | $10^9 r_m$/ mols$^{-1}$ gcat$^{-1}$ | $E_a$/kJ mol$^{-1}$ [a] | Conversion $T_{50}$/K |
|---|---|---|---|---|---|
| 10V10 | 3.7 | 34 | 4000 | 73 | 424 |
| 10V8 | 3.3 | 40 | 3600 | 72 | 421 |
| 10V6 | 2.0 | 28 | 2200 | 60 | 421 |
| 10V3 | 1.4 | 31 | 1500 | 60 | 428 |
| 10V2 | 0.8 | 30 | 870 | 55 | 443 |
| 5V6 | 0.9 | 6.4 | 510 | 69 | 468 |
| 2V6 | 0.03 | 0.08 | 6.8 | 92 | 568 |
| 0V6 | — | — | — | — | Above 700 K |
| 10V4Si6 | 1.5 | 21 | 1700 | 62 | 429 |
| 10V4Si3 | 1.1 | 25 | 1300 | 62 | 433 |
| 10V7Si6 | 1.4 | 19 | 1550 | 60 | 436 |
| 10V7Si3 | 1.2 | 29 | 1300 | 62 | 426 |
| 5V3 | 3.2 | 36 | 1800 | 77 | 443 |

[a] Maximal error 5%.

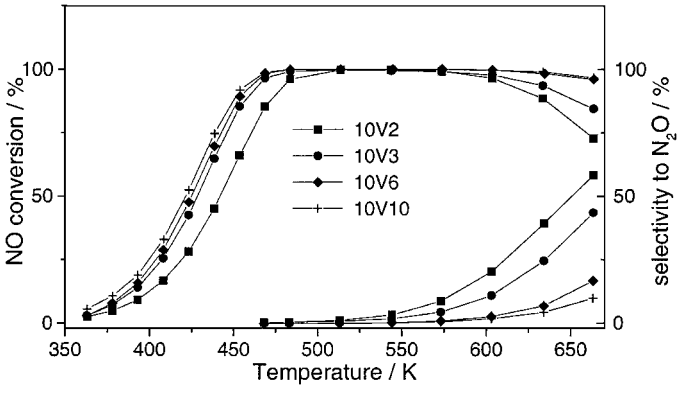


**FIG. 11.** NO conversion (left axis, upper curves) and selectivity to $N_2O$ (right axis) as a function of temperature for 10 wt% vanadia samples. Oxygen flow rates vary from 2 to 10 L/min.

silica reduced the TOF by 30%; no further deactivation was observed if more silica (7 wt%) was added. The effect of silica was the same in both flames. Figure 13 shows the Arrhenius plots for a series of catalysts prepared with different oxygen flow rates. The activation energy was constant at 60 kJ/mol for low oxygen flow rates (10V2, 10V3, and 10V6), but increased to 73 kJ/mol for high oxygen flow rates (10V10).

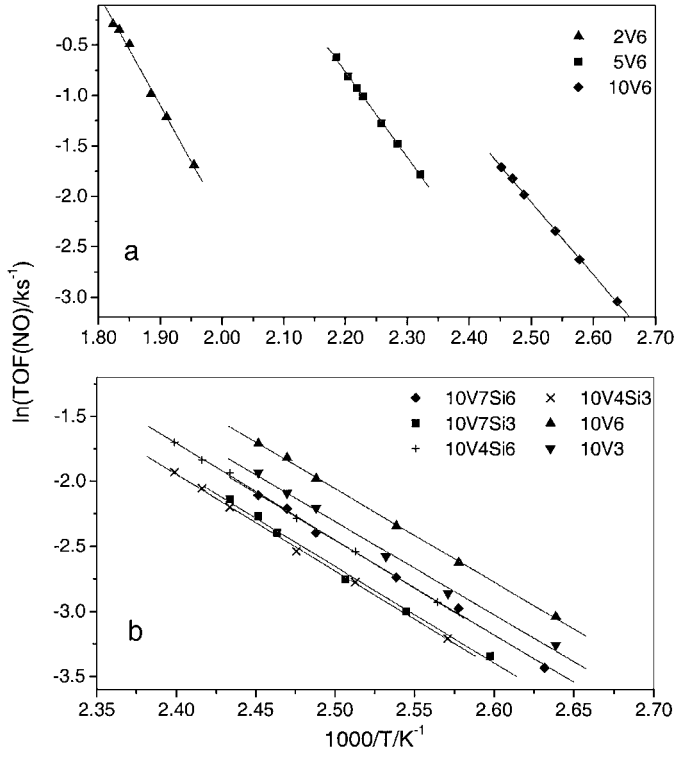


**FIG. 12.** Catalytic behavior (Arrhenius plot) in SCR of samples with different composition. (a) Influence of vanadia content, and (b) influence of silica content.

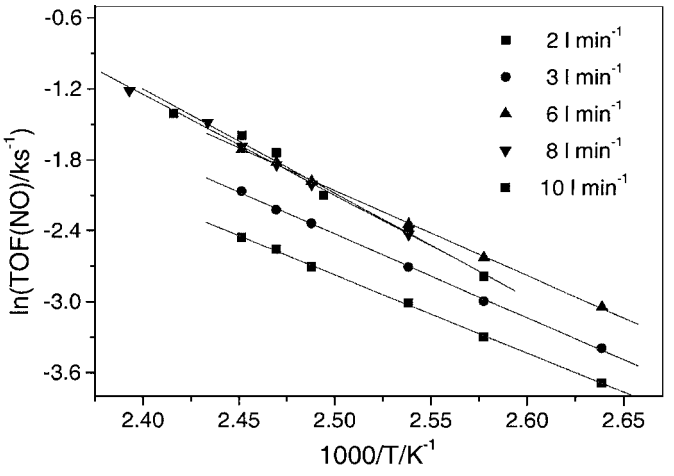


**FIG. 13.** Influence of oxygen flow rate used in preparation on catalytic behavior (Arrhenius plot) in SCR.

## 4. DISCUSSION

### *4.1. Structural and Textural Properties*

The HRTEM pictures show that titania and vanadia form nonaggregated spherical particles in a methane oxygen diffusion flame. The small size of these particles leads to large specific surface areas. The trend observed in Fig. 3 can be rationalized in terms of the particle formation process. Titania vapor condenses in the flame to small liquid droplets. Due to their high surface tension they are perfectly spherical and contain no micropores, as previously reported by Miquel *et al.* (9). Most particles consist of one single crystallite because grain boundaries are ruled out by solid diffusion. If two particles collide, they coalesce and form one bigger particle. This process is active throughout the hot part of the flame and increases the average particle size and therefore reduces the specific surface area. Adding more oxygen to the flame accelerates the oxidation process as well as fuel–oxidant mixing. This leads to shorter flames (see Table 1 and Fig. 2), and steeper temperature gradients (1). Less time for coagulation and coalescence leads to smaller particles. The size of the titania particles may therefore be altered by adjusting the oxygen flow rate (14). The composition of the particles has little influence on their specific surface area (Fig. 3). $V_2O_5$ is very volatile (27, 28) and is expected to condense on the titania particles only in the colder top part of the flame. The additional thin vanadia layer does not affect the specific surface area. This has already been observed in grafting processes (21).

All flame-made powders contain mainly anatase (see Fig. 5), which is reported to lead to good spreading of vanadia on titania (29). This stays in contrast to the powders produced by Miquel *et al.* (9), which contained mainly rutile. Even though silica has been reported to inhibit rutile formation (30), no influence of silica can be found in XRD.

In sol-gel catalysts, silica is generally expected to hinder solid diffusion and keep small titania crystallites apart. The TEM image in Fig. 7 shows that silica forms a separate phase and does not cover or mix with the titania which stays in accord with the phase diagram of silica/titania (31). It is clear that this remote silica cannot affect the crystallinity of titania. Vanadia has no influence on the crystallinity of the flame-made titania, even though the temperature at which anatase sintering and phase transformation to rutile occur is sensitive to the vanadia content (32). This supports the assumption that vanadia only covers the titania after the particles are crystallized. The formation of an interstitial solution of V(4+) in the titania lattice can be excluded based on the hydrogen consumption in TPR (Table 2). XPS (Table 3), Raman spectra (Figs. 8 and 9), and laser ablation ICP MS (Table 1) show that the vanadia is dispersed on the titania surface. No individual vanadia particles are formed. This morphology guarantees exceptional accessibility to the vanadia sites from the gas phase. Sanati *et al.* (33) found that mechanical mixtures of vanadia and titania form well-dispersed vanadia clusters upon heat treatment at 450°C in air for 36 h. Machej *et al.* (34) concluded that the distribution of vanadia is entirely driven by thermodynamics and is almost independent of the preparation method. Obviously, this is even true for flame-made particles. The spreading of the vanadia and the establishment of equilibrium between different vanadia phases must be very fast processes because reaction times in the flame are short, typically 5 to 50 ms.

Raman spectroscopy shows that flame-made catalysts with 5 and 10 wt% vanadia contain the same type of vanadia species as classically prepared catalysts (Figs. 8 and 9). At high vanadia loading, crystalline vanadia is visible in Raman spectroscopy (35), but crystallites are too small to be detected in XRD. The theoretical monolayer coverage (36, 37) corresponds to 12.3 and 16.4 wt% vanadia for 10V8 and 10V10, respectively. Both catalysts are in the submonolayer region but show some crystalline $V_2O_5$ in Raman spectroscopy. This is generally not the case for classically prepared catalysts (38). Interestingly, the vanadia of 2V6 with a surface loading of only 2.5 $\mu$mol/m$^2$ does not form monomers but predominantly condensed vanadia species (Fig. 9). This result disagrees with the usual redistribution and vanadia spreading of classical catalysts and may be attributed to the complete dehydration of the titania surface in the flame.

### 4.2. Catalytic Behavior

NO conversion strongly depends on the vanadia loading (Fig. 10). The TOF of flame-made catalysts increases by a factor of 30 when increasing the vanadia loading from 2.5 to 7 $\mu$mol/m$^2$. This behavior is in line with wet chemical preparation methods (39). Wachs *et al.* (40) observed a fivefold

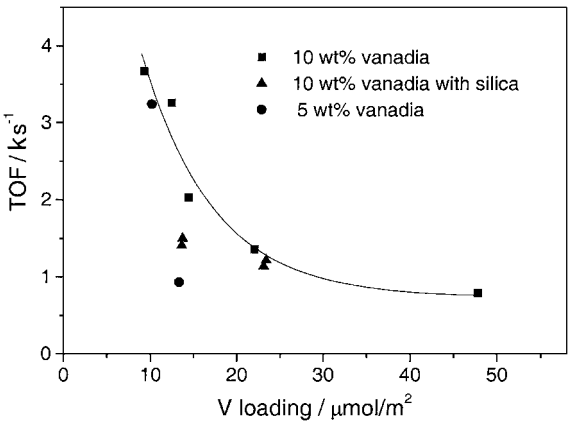


**FIG. 14.** Influence of the vanadia loading on SCR activity for differently prepared materials.

increase in TOF for catalysts prepared by incipient wetness impregnation of titania (Degussa P 25, 50 m$^2$/g) when going from 1 to 6 wt% vanadia. The data of Baiker *et al.* (41) show that the TOF increases by a factor of 20 to 30 when the vanadia coverage increases from 2 to 6 $\mu$mol/m$^2$. The increase is generally attributed to the higher specific activity of polymeric vanadate species (42) or the accompanying increase in Brønsted acid sites with vanadia surface coverage (43). The vanadia species appearing in flame-made catalysts are essentially the same as in classical catalysts. Optimal activity is achieved at a surface loading of 10 $\mu$mol/m$^2$; see Fig. 14. This value seems to be independent of the flame used during preparation as samples 10V10 and 5V3, which were prepared with two different flames, indicate. At high vanadia loading, the TOF decreases continuously, but the activity per surface stays almost constant; see Table 4. This is attributed to the reduced accessibility of vanadia in crystallites and covered layers. The occurrence of a maximum in TOF for different loadings was reported by Amiridis *et al.* (44) and Wachs *et al.* (45). The apparent activation energy is very high in low vanadia samples (Table 4) and decreases with increasing loading (46). In contrast to other catalysts, highly active catalysts (10V10, 10V8, 5V3) exhibit higher energy of activation than classical catalysts. Adding silica leads to some deactivation (Fig. 12b) but no influence on the activation energy is found. This is in line with the fact that silica covers part of the active surface and therefore lowers the number of active sites per mass of catalyst. The lowering of activity upon addition of silica has also been observed with sol-gel-derived $V_2O_5$ on $TiO_2$–$SiO_2$ catalysts (47).

The selectivity to $N_2$ depends on the surface vanadia loading. At high loading, up to 30% $N_2O$ are formed at 623 K (Fig. 11). The best catalyst 5V3 produces less than 1% $N_2O$ at 623 K. At the same time NO conversion is better than 99%. Flame-made catalysts compare favorably to catalysts prepared by incipient wetness impregnation and grafting, see Table 5.

**TABLE 5**

**Comparison of Different Catalysts**

| Sample | TOF (423 K)/ $ks^{-1}$ | TOF (473 K)/ $ks^{-1}$ | $S(N_2)$/% at 623 K |
|---|---|---|---|
| 5V3 | 0.31[a] | 3.2[b] | 99[a] |
| 10V10 | 0.41[a] | 3.7[b] | 96[a] |
| 4.3 wt% V (grafted, (21)) | 0.48[a] | 3.0[b] | — |
| 6 wt% V (impr., (45)) | — | 1.7[a] | 78[a] |

[a] Measured values.
[b] Calculated values using $E_a$ (Table 2).

## 5. CONCLUSIONS

Flame aerosol synthesis has been shown to successfully produce vanadia on agglomerated titania nanoparticles of regular spherical shape. Compared to catalysts from conventional methods, the texture of flame-made catalysts shows minimal porosity at high specific surface area. No indication for the formation of an interstitial solution of vanadium inside the titania lattice is found. Vanadia spreads out well and homogenous distributions are obtained. The powders exhibit excellent activity for SCR of NO by $NH_3$. These materials show a similar overall behavior to powder catalysts prepared by classical methods. The activity, expressed as the turnover frequency, increases strongly with vanadia loading in the submonolayer region. A decrease in TOF and an increase in $N_2O$ production is observed for higher vanadia loading. In contrast to catalysts derived from classical preparation methods, predominant formation of condensed vanadate species is already observed at low loading. High activity correlates with high apparent activation energy values. Addition of silica lowers the activity, presumably by covering part of the titania surface.

## ACKNOWLEDGMENTS

We thank P. Fabrizioli (ETH) for help with catalytic measurements, Professor Dr. D. Guenther (ETH) for laser ablation ICP MS, M. Hauer (PSI, Villigen) for the Raman measurements, and Dr. F. Krumeich (ETH) for the HRTEM images. Financial support granted by the ETH Gesuch Nr. 33/99-2 is kindly acknowledged.

## REFERENCES

1. Pratsinis, S. E., *Prog. Energy Combust. Sci.* **24**, 197 (1998).
2. Wooldridge, M. S., *Prog. Energy Combust. Sci.* **24**, 63 (1998).
3. Ulrich, G. D., *Chem. Eng. News* **62**, 22 (1984).
4. Moser, W. R., *in* "Catalytic Selective Oxidation" (S. T. Oyama and J. W. Hightower, Eds.), ACS Symposium Series, Vol. 523, 1993.
5. Michalakos, P. M., Bellis, H. E., Brusky, P., Kung, H. H., Li, H. Q., Moser, W. R., Partenheimer, W., and Satek, L. C., *J. Am. Chem. Soc.* **34**, 1994 (1995).
6. Moser, W. R., *Catal. Today* **21**, 157 (1994).
7. Moser, W. R., *Chem. Eng. Comm.* **83**, 241 (1989).
8. Miquel, F. P., and Katz, J. F., *J. Mater. Res.* **9**, 746 (1994).
9. Miquel, F. M., Hung, C. H., and Katz, J. L., *J. Mater. Res.* **8**, 2404 (1993).
10. Hung, C. H., and Katz, J. L., *J. Mater. Res.* **7**, 1861 (1992).
11. Fotou, G. P., Vemury, S., and Pratsinis, S. E., *Chem. Eng. Sci.* **49**, 4939 (1994).
12. Fotou, G. P., and Pratsinis, S. E., *Chem. Eng. Comm.* **151**, 251 (1996).
13. Bosch, H., and Janssen, F., *Catal. Today* **2**, 369 (1988).
14. Pratsinis, S. E., Zhu, W., and Vemury, S., *Powder Technol.* **86**, 87 (1996).
15. Briesen, H., Fuhrmann, A., and Pratsinis, S. E., *Chem. Eng. Sci.* **53**, 4105 (1998).
16. Moulder, J. F., Stickle, W. F., Sobol, P. E., and Bomben, K. D., "Handbook of X-Ray Photoelectron Spectroscopy" (J. Chastain, Ed.), Perkin–Elmer Corp., Eden Prairie, MN, 1992.
17. Scofield, J. H., *J. Electron Spectr. Relat. Phenom.* **8**, 129 (1976).
18. Guenther, D., Frischknecht, R., Heinrich, C. A., and Kahlert, J. H., *J. Anal. Atomic Spectr.* **12**, 939 (1997).
19. Koeppel, R. A., Nickl, J., and Baiker, A., *Catal. Today* **20**, 45 (1994).
20. Engweiler, J., and Baiker, A., *Appl. Catal.* **120**, 187 (1994).
21. Reiche, M. A., Hug, P., and Baiker, A., *J. Catal.* **192**, 400 (2000).
22. Sanchez, C., Livage, J., and Lucaceau, G., *J. Raman Spectrosc.* **12**, 68 (1982).
23. Schraml-Marth, M., Wokaun, A., and Baiker, A., *Fres. J. Anal. Chem.* **341**, 87 (1991).
24. Cristiani, C., Forzatti, P., and Busca, G., *J. Catal.* **116**, 586–589 (1989).
25. Oyama, S. T., Went, G. T., Lewis, K. B., Bell, A. T., and Somorjai, G. A., *J. Phys. Chem.* **93**, 6789 (1989).
26. Went, G. T., Oyama, S. T., and Bell, A. T., *J. Phys. Chem.* **94**, 4240 (1990).
27. Wickert, K., *Brennstoff-Waerme-Kraft* **11**, 266 (1959).
28. Neugebrauer, J., *Acad. Sci. Hung.* **37**, 247 (1963).
29. Haber, J., Machej, T., Serwicka, E. M., and Wachs, I. E., *Catal. Lett.* **32**, 101 (1995).
30. Vemury, S., and Pratsinis, S. E., *J. Am. Ceram. Soc.* **78**, 2284 (1995).
31. De Vries, R. C., Roy, R., and Osborn, E. F., *Trans. B. Ceram. Soc.* **53**, 531 (1954).
32. Oliveri, G., Busca, G., and Lorenzelli, V., *Mater. Chem. Phys.* **22**, 511 (1989).
33. Sanati, M., Wallenberg, L. R., Andersson, A., Jansen, S., and Tu, Y. P., *J. Catal.* **132**, 128 (1991).
34. Machej, T., Haber, J., Turek, A. M., and Wachs, I. E., *Appl. Catal.* **70**, 115 (1991).
35. Khodakov, A., Olthof, B., Bell, A. T., and Iglesia, E., *J. Catal.* **181**, 205 (1999).
36. Bond, G. C., and Tahir, S. F., *Appl. Catal.* **71**, 1 (1991).
37. Bond, G. C., Zurita, J. P., Flamerz, S., Mars, P., and Gellings, P., *Appl. Catal.* **22**, 361 (1986).
38. Wauthoz, P., Ruwet, M., Machej, T., and Grange, P., *Appl. Catal.* **149** (1991).
39. Baiker, A., Dollenmeier, P., Glinski, M., and Reller, A., *Appl. Catal.* **35**, 351 (1987).
40. Wachs, I. E., Deo, G., Weckhuysen, B. M., Andreini, A., Vuurman, M. A., deBoer, M., and Amiridis, M. D., *J. Catal.* **161**, 211 (1996).
41. Baiker, A., Handy, B., Nickl, J., Schraml-Marth, M., and Wokaun, A., *Catal. Lett.* **14**, 89 (1992).
42. Went, G. T., Leu, L. J., Rosin, R. R., and Bell, A. T., *J. Catal.* **134**, 492 (1992).
43. Topsoe, N. Y., Dumesic, J. A., and Topsoe, H., *J. Catal.* **151**, 241 (1995).
44. Amiridis, M. D., Wachs, I. E., Deo, G., Jehng, J.-M., and Kim, D. S., *J. Catal.* **161**, 247 (1996).
45. Wachs, I. E., Deo, G., Weckhuysen, B. M., Andreini, A., Vuurman, M. A., de Boer, M., and Amiridis, M. D., *J. Catal.* **161**, 211 (1996).
46. Amiridis, M. D., and Solar, J. P., *Ind. Eng. Chem. Res.* **35**, 978 (1996).
47. Reiche, M. A., Ortelli, E., and Baiker, A., *Appl. Catal. B* **23**, 187 (1999).